Clustering and flow around a sphere moving into a grain cloud

A. Seguin, A. Lefebvre-Lepot, S. Faure and P. Gondret

Regular Article

Clustering and flow around a sphere moving into a grain cloud

A. Seguin[1,4,a], A. Lefebvre-Lepot[2], S. Faure[3], and P. Gondret[1]

[1] Laboratoire FAST, Université Paris-Sud, CNRS, Université Paris-Saclay, F-91405, Orsay, France
[2] CMAP, CNRS, Ecole Polytechnique, Université Paris-Saclay, F-91128, Palaiseau, France
[3] LMO, CNRS, Université Paris-Sud, Université Paris-Saclay, F-91405, Orsay, France
[4] SPEC, CEA, CNRS, Université Paris-Saclay, F-91191, Gif-sur-Yvette, France

Abstract. A bidimensional simulation of a sphere moving at constant velocity into a cloud of smaller spherical grains far from any boundaries and without gravity is presented with a non-smooth contact dynamics method. A dense granular "cluster" zone builds progressively around the moving sphere until a stationary regime appears with a constant upstream cluster size. The key point is that the upstream cluster size increases with the initial solid fraction ϕ_0 but the cluster packing fraction takes an about constant value independent of ϕ_0. Although the upstream cluster size around the moving sphere diverges when ϕ_0 approaches a critical value, the drag force exerted by the grains on the sphere does not. The detailed analysis of the local strain rate and local stress fields made in the non-parallel granular flow inside the cluster allows us to extract the local invariants of the two tensors: dilation rate, shear rate, pressure and shear stress. Despite different spatial variations of these invariants, the local friction coefficient μ appears to depend only on the local inertial number I as well as the local solid fraction, which means that a local rheology does exist in the present non-parallel flow. The key point is that the spatial variations of I inside the cluster do not depend on the sphere velocity and explore only a small range around the value one.

1 Introduction

The response of a granular material to a mechanical perturbation by the motion of a solid object at its surface or in its bulk is a fundamental issue in many fields. For instance, in civil engineering, the resistance of soils to the penetration or extraction of stakes and piles is an important point for the safety of structures. In biophysics, the understanding of animal locomotion in sand [1] may inspire new robotics in very different situations, from agricultural to military machinaries. And in geophysics, the collision phenomena in the impacts of meteorits on planets or asteroids [2], or in the formation of protoplanetary disks from dust particles [3], are the basic elementary processes that need to be taken into account for a better understanding of the evolution of the universe. In all these cases, the complex rheology of the granular material plays a key role and needs to be well-understood, which is particularly hard when the packing is dense with a high solid fraction ϕ close to the so-called liquid/solid or jamming transition [4–6]. Different rheological laws have been proposed for dense granular flows, such as the so-called $\mu(I)$ rheology which relates the local friction coefficient μ and the local packing fraction ϕ to the dimensionless inertial number I [7]. This local rheology has been built from

numerical and experimental results obtained in stationary parallel flows: Couette flow between two close parallel walls in relative motion [8] or thin flows down inclined planes [9]. Although such a rheological law may give some good results in quasi-steady and quasi-parallel flows [10–14], its validity for strongly non-parallel flow still needs to be addressed. Even in simple parallel shear flows, the existence of such a local rheology and the influence of solid walls is still under investigation [15,16]. As a matter of fact, the presence of far boundaries such as fixed or mobile solid walls has shown to have strong and non-elucidated actions in different situations [17–19]. To examine this important question, one must have access simultaneously to the strain and stress fields in the bulk flow. Different experimental tools have been developed to measure both the kinematic properties of granular flows and the force contact network such as image correlation techniques [19, 20] or light backscattering [21] for the former, and non-linear acoustics [22], photoelastic techniques [5,23–26], or even X-ray or neutrons diffraction [27] for the latter. In addition to these remarkable experimental tools, discrete numerical techniques is now a powerful tool to investigate deeply the complex granular flows [8,10,15,16,28,29].

The object of the present paper is to investigate the local rheology of granular matter in a strongly non-parallel flow around a moving sphere without any gravity field and

a e-mail: `antoine.seguin@u-psud.fr`

far from any other boundaries. We use for this a recent powerful numerical method described in sect. 2 to investigate such a sphere motion within a bidimensional cloud of spherical particles initially at rest with a solid fraction ϕ_0 far below the jamming point. The size of the dense cluster that builds progressively around the moving sphere is characterized in sect. 3 and the corresponding stationary drag force in sect. 4. A local analysis of the stress and strain rate in the stationary flow that arises in the dense cluster around the sphere intruder is made in sect. 5 and the local rheology is finally examined in sect. 6.

2 Numerical model

In the Discrete Elements Methods (DEM) used to simulate granular flows, two classes of numerical methods can be distinguished. "Explicit methods", also called "smooth methods", consider that collision forces can be explicitly expressed as a function of the configuration of the system as, *e.g.*, for a spring network. This leads to very stiff Ordinary Differential Equations which impose to use small time steps in the simulations. The numerical method we use here belongs to the class of "Non-Smooth Contact Dynamic methods" [30,31] and is described in details in [32]. In these methods, impenetrability is expressed by writing that the gap between solid bodies should remain positive and the contact force is an unknown of the problem. This leads to robust numerical schemes and allows to use larger time steps. Here, we simulate the motion of dissipative rigid spheres with a non-elastic impact law (zero restitution coefficient for the collisions) but without any static nor dynamic friction between the spheres.

The present simulation configuration is as follows. The granular assembly is contained in a rectangular box of size L_x along the x streamwise direction of motion and L_y in the transverse direction y with $(x, y) = (0, 0)$ at the center of the box. It is made of slightly polydisperse spherical grains of mean diameter d_g and density ρ, with a uniform size distribution in the range $0.9d_g$ to $1.1d_g$ in order to avoid any possible crystallization during the simulation. A sphere of larger diameter $d = 10d_g$, which is initially placed at one side of the rectangular box at $x = -L_x/3$ and $y = 0$, is then moved at constant velocity V_0 in the x direction toward the opposite side. The interaction between the grains and the moving sphere as well as between the grains and the walls is solved using the same law as for the grain-grain interaction.

To prepare the granular medium at the initial solid fraction $\phi_0 = N(\pi d_g^2/4)/(L_x L_y - \pi d^2/4)$, we pick randomly N centers of non-intersecting spheres of diameter d_g in the box of size $L_x \times L_y = 1100d_g \times 800d_g$, and apply a random force on the grains to ensure a uniform spatial configuration of spheres without any contact force. For required ϕ_0 values higher than 0.7, an initial $\phi_0 = 0.7$ configuration is slightly compacted by slightly moving one side wall of the box thus slightly decreasing L_x to reach the required $\phi_0 > 0.7$, before a random force is applied on the grains to obtain again a uniform spatial distribution of grains without any contact. For the highest

range of the solid fraction built here $(0.7 \leqslant \phi_0 \leqslant 0.75)$, the length of the box thus lies in the reduced range $1030 \leqslant L_x/d_g \leqslant 1100$. It is worth noting that all the explored initial solid configuration are far below the jamming point which is known to be at the packing fraction $\phi_J \simeq 0.84$ in 2D [24,33].

Starting the intruder sphere motion, the numerical solver gives the velocity v_m of each particle m and the contact force f_{mn} exerted by particle m on particle n (which is zero if particles m and n are not in contact). The velocity field v at any point of the domain is computed using an interpolation of the v_m values onto a Cartesian grid of step $\Delta x = \Delta y = 0.05d_g$. Besides, for each particle m, one can define the corresponding stress tensor:

$$\sigma^m = \frac{4}{\pi d_g^2} \sum_n e_{mn} \otimes f_{nm},$$

where e_{mn} is the unit vector giving the direction from the center of particle m toward the center of particle n and $\otimes$ is the vector outer product. The stress tensor σ at any point of the domain is then computed by interpolating the σ^m values on the same Cartesian grid as for the velocity field v.

The local solid fraction ϕ_m around each particle m is first computed using a Voronoi tesselation, and the local solid fraction ϕ at any point of the domain is then computed by interpolating the ϕ_m values on the same Cartesian grid as for v and σ.

From the velocity field v and the stress tensor field σ, one can define the following quantities of interest in the whole domain:

- The pressure $p = -\frac{1}{2} \sum_k \sigma_{kk}$, defined by the opposite of the mean normal stress.
- The shear stress $\tau = \sqrt{\frac{1}{2} \sum_{i,j} (\sigma_{ij} + p\delta_{ij})^2}$, defined by the mean deviatoric component of the stress tensor, where δ_{ij} is the Kronecker symbol.
- The dilation rate $\dot{\varepsilon} = \frac{1}{2} \sum_k D_{kk}$, defined by the mean normal strain, where $D_{ij} = (\partial_i v_j + \partial_j v_i)/2$ is the strain rate tensor.
- The shear rate $\dot{\gamma} = \sqrt{\frac{1}{2} \sum_{i,j} (D_{ij} - \dot{\varepsilon}\delta_{ij})^2}$, defined by the mean of the deviatoric component of the strain rate tensor.

Note that the 1/2 factor for p and $\dot{\varepsilon}$ arises from the present bidimensionnal configuration.

The drag force F exerted by the grains on the intruder can be calculated as $F = -\sum_m f_{m0} \cdot e_x$, where f_{m0} is the contact force exerted by particle m on the intruder and e_x is the unit vector along the x direction of motion.

In the following, d_g will be chosen as unit of length and V_0 as unit of velocity, so that d_g/V_0 will be chosen as unit of time. As no gravity acts and no external pressure is imposed in the present configuration, there is no pressure scale other than ρV_0^2, which will thus be chosen as the unit of stress and $\rho d_g^2 V_0^2$ as the unit of force. The spatial variation of each local quantities will be presented in the polar coordinates (r, θ) adapted to the geometry, where θ is the angle relative to the x direction of motion and
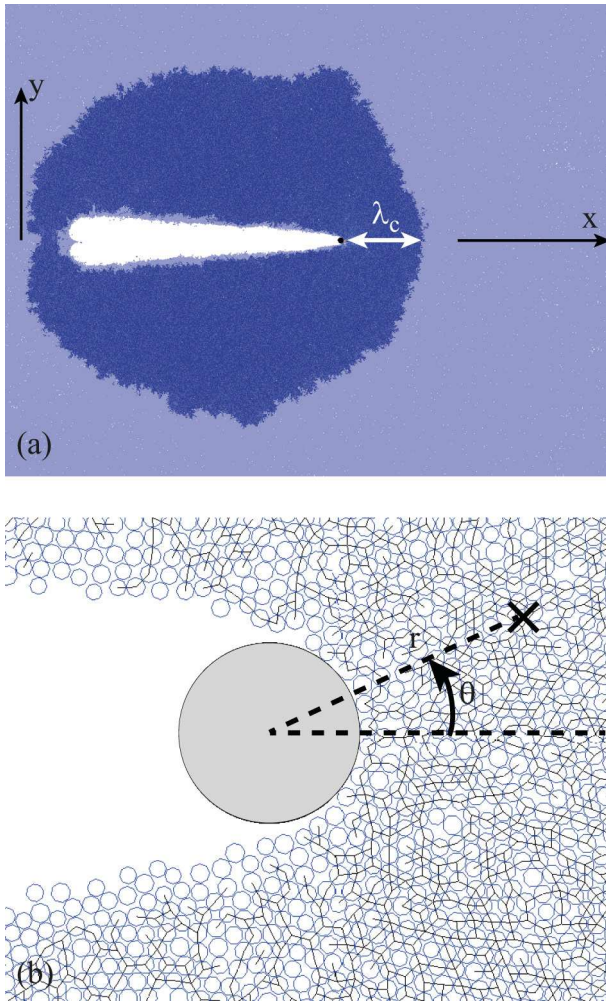
Fig. 1. (Color online). (a) Snapshot of a simulation for the initial solid fraction $\phi_0 = 0.75$. The length λ_c corresponds to the cluster size in front of the sphere moving from left to right. (b) Same snapshot but zoomed in around the sphere intruder. The black lines indicate non-zero contact forces between touching grains.

r the radial position relative to the moving sphere center (fig. 1b).

3 Dynamical clustering

As the intruder starts moving, it perturbs progressively the initial grain assembly and a dense cluster zone of touching grains grows around as illustrated in fig. 1. In this figure, the grains are drawn as open disks in light gray (light blue online) and non-zero contact forces between touching grains are drawn as black lines connecting the grain centers. The open disks and black lines can be seen individually in fig. 1b that displays only a zoomed part close around the moving intruder. In fig. 1a that displays the entire domain, touching grains appear in dark gray (dark blue online). The dense cluster exhibits an ovoid shape which does not touch any limiting walls, so that the cluster is surrounded by non-contacting grains at the

initial fraction ϕ_0 which have not moved yet. The position $r_c(\theta, t)$ of the corresponding front delimiting the inner perturbed cluster zone to the outer unperturbed zone is extracted from the simple criterion $p(r > r_c) = 0$ for each θ. A triangular zone with no grain inside, thus appearing in white in fig. 1a, exists in the wake of the intruder as already reported and analyzed in details by [34] in bidimensional experiments. In the present paper, we only focus on the cluster zone upstream the intruder ($-\pi/2 \lesssim \theta \lesssim \pi/2$) which is the key region where the drag force originates, with high stresses and strain rates inside. The upstream extension of the cluster $\lambda = r_c - d/2$ is averaged in the small θ range $-5° < \theta < 5°$ around the x-direction of motion. As in one dimensional experiments where a straight rake starts moving [35], we observe that the front position λ moves away linearly in time, with a velocity that is proportional to the intruder velocity and increases with the initial fraction ϕ_0. But in contrast to the one-dimensional configuration of [35], this regime is here only transient until a steady regime is reached with a constant value λ_c. This steady regime appears when the grain flux upstream the intruder is balanced by the grain flux on the intruder sides which can not occur in the one-dimensional configuration of [35] as no grains can circumvent the rake. In the following, we restrict our study to this steady state regime which allows time averaging of the different measured quantities.

The steady size of the dynamic cluster that appears around the moving sphere is observed to increase with ϕ_0 (see fig. 2a) from only a few grains at low ϕ_0 (*e.g.* $\lambda_c \simeq 3d_g$ at $\phi_0 = 0.3$) to many grains at high ϕ_0 (*e.g.*, $\lambda_c \simeq 53dg$ at $\phi_0 = 0.7$). The radial variation of the local solid fraction $\phi(r, 0)$ in the streamwise direction $\theta = 0$ in front of the moving sphere is displayed in fig. 2b for different initial solid fractions ϕ_0. For large enough ϕ_0 ($\phi_0 \gtrsim 0.6$), ϕ reaches a plateau value $\phi_p \simeq 0.83$ in the cluster except close to the intruder where ϕ decreases down to about 0.75 and near the front where ϕ decreases down to ϕ_0. This plateau value ϕ_p is not reached for low enough ϕ_0 ($\phi_0 \lesssim 0.6$). As demonstrated by the log-log inset plot of fig. 2a, λ_c diverges at the approach of a critical value ϕ_c with the scaling $\lambda_c/d_g = \alpha(\phi_c - \phi_0)^{-2}$ where $\alpha = 1.5 \pm 0.3$ and $\phi_c \simeq 0.85 \pm 0.01$. The critical value ϕ_c found here is very close to the jamming point ϕ_J reported in other studies [24,33]. Note that the local solid fraction ϕ does not vary significantly with θ in a large azimutal range as shown by the inset of fig. 2b.

4 Drag force

In the present simulations where no gravity acts and no external pressure is imposed from any external boundary, no stress scale exists except the kinetic pressure ρV_0^2 arising from collision processes. We have checked that the drag force F exerted by the grains on the moving sphere indeed scales as ρV_0^2 for any velocity range V_0. The present regime corresponds therefore to the inertial high velocity regime found by [36,37] in their bidimensional experiments of a disk dragged within a monolayer of steel beads and also
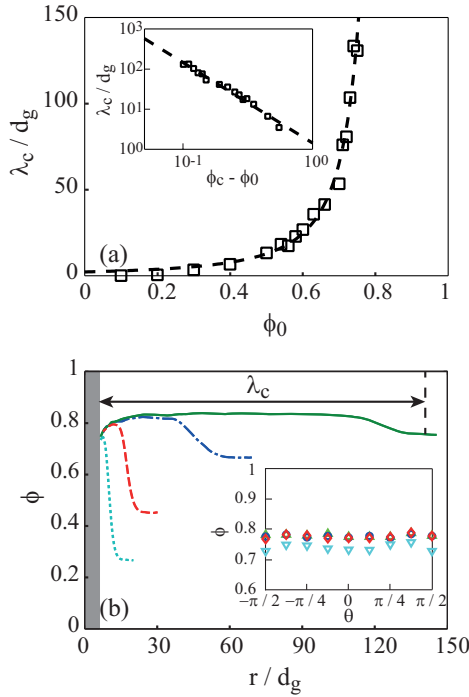
Fig. 2. (Color online). (a) Cluster size λ_c as a function of the initial solid fraction ϕ_0. ($\square$) Numerical results and (- - -) best fit of equation $\lambda_c/d_g = \alpha(\phi_c - \phi_0)^{-2}$ with $\alpha = 1.44$ and $\phi_c = 0.85$. Inset: Log-log plot of λ_c/d_g vs. $\phi_c - \phi_0$. (b) Radial variation of the local solid fraction ϕ in the direction of motion ($\theta \simeq 0$) for different initial solid fractions $\phi_0 = 0.3 (\cdots)$, 0.5 (- - -), 0.7 (- · -), 0.75 (——). Inset: Azimutal variations of ϕ at the radial distance $r \simeq 8d_g$ for $\phi_0 = 0.3 (\triangledown)$, 0.5 ($\diamond$), 0.7 ($\circ$), 0.75 ($\triangle$).

found by [29] in their numerical simulations of a bidimensional assembly of disks with no friction with the bottom plate. In our simulation, we do not observe any quasistatic regime at low velocity where the drag force would be velocity independent or would depend only weakly on the velocity. The existence of such a quasi-static regime which is the most often seen regime [19,20,38] arises from the existence of another natural scale of pressure in the system which may come either from gravity or from wall friction.

Figure 3a shows that the present normalized drag force $F/\rho d_g^2 V_0^2$ increases with the initial solid fraction ϕ_0 in a linear way even at high ϕ_0 when approaching ϕ_c. Indeed, a linear fit $F/\rho d_g^2 V_0^2 = K\phi_0$ with $K = 4.9 \pm 0.1$ passes quite well through the all data range. Thus, F does not seem to diverge at the approach of ϕ_c in contrast to the cluster size λ_c. Hence, if the increase of F may be related to the increase of λ_c at small ϕ_0, this is not the case at high ϕ_0: F remains finite whereas λ_c diverges. Figure 3b displays the evolution of the drag force F with the cluster size λ_c. From the previous simple scalings $\lambda_c/d_g = \alpha(\phi_c - \phi_0)^{-2}$ and $F/\rho d_g^2 V_0^2 = K\phi_0$ found for the ϕ_0 dependence of F and λ_c, one can infer the simple scaling $F/\rho V_0^2 d^2 = K[\phi_c - (\alpha d_g/\lambda_c)^{1/2}]$. The corresponding law passes quite well through the data as shown in fig. 3b where the normalized drag force is expected to saturate at the value $K\phi_c \simeq 4$ when λ_c/d_g goes to infinity
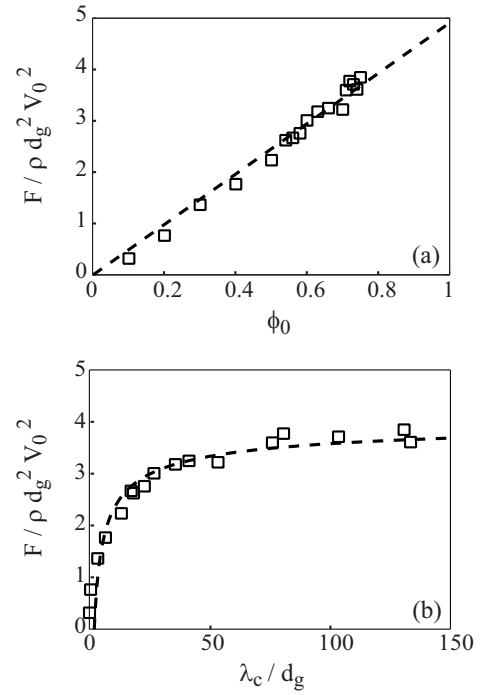

Fig. 3. Normalized drag force $F/\rho d_g^2 V_0^2$ as a function of (a) the initial solid fraction ϕ_0 fitted by the linear equation $F/\rho d_g^2 V_0^2 = K\phi_0$ with $K = 4.9$ (- - -), and (b) as a function of the dimensionless cluster extension λ_c/d_g fitted by equation $F/\rho d_g^2 V_0^2 = 4.9[0.85 - (1.44 d_g/\lambda_c)^{1/2}]$ (- - -).

for ϕ_0 approaching ϕ_c. The present saturation of the drag force at high ϕ_0 is a strong result. Indeed, the present finding is different from the scaling prediction of [37] based on their experimental measurements where the drag force F seems to diverge for initial solid fractions approaching a critical value. It is also different from the divergence of the drag force observed in the numerical simulations of [29]. But the present finding is consistent with theoretical predictions of dense packing of spheres where the yield stress is not expected to diverge when the system crosses the jamming point [39]. The reason why we do not observe any divergence for the force may be explained by the fact that the grains at the outer limit of the growing cluster do not touch any limit boundary in our simulations.

5 Local invariants

Let us now focus on the flow around the moving intruder. As there is no grain motion and no contact force outside, we will only consider the dense cluster zone in the study of the invariants of both the local strain rate tensor and the local stress tensor: the local dilation rate $\dot\varepsilon$ and shear rate $\dot\gamma$ together with the local pressure p and shear stress τ. Figures 4a and b display the spatial evolution of the normalized dilation rate $\dot\varepsilon d_g/V_0$ as a function of the normalized radial distance r/d_g in front of the moving sphere ($\theta \simeq 0$) and as a function of the azimuthal angle θ close to the moving sphere ($r \simeq 8d_g$) for three values of the initial solid fraction ϕ_0 with a significant cluster size ($\lambda_c > 10d_g$). We can see in fig. 4a that $\dot\varepsilon d_g/V_0$ is about zero in the overall cluster except near the cluster rim at the front where a

Fig. 5. (Color online). (a) Radial and (b) azimutal variation of the inertial number I in the dense zone around the intruder for different initial solid fractions ϕ_0. Same symbols as in fig. 4.
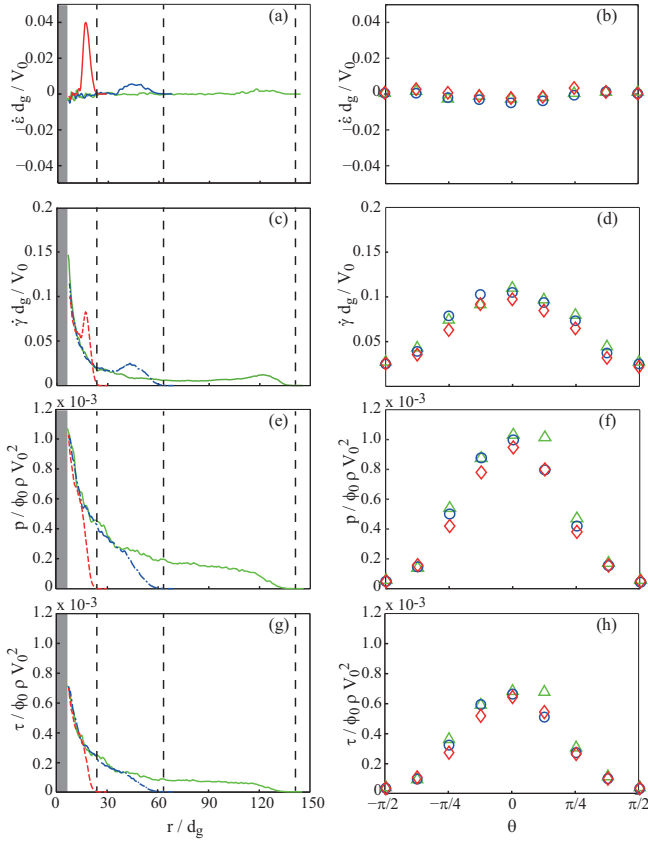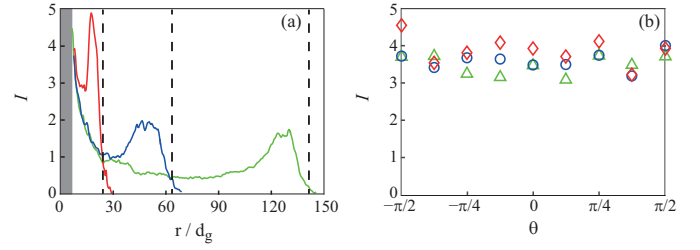

Fig. 4. (Color online). Spatial evolution of the four invariants of the strain rate and stress tensors around the intruder for different initial solid fractions $\phi_0 = 0.5$ (- - -, $\diamond$), 0.7 (- · -, $\circ$), 0.75 (—, $\triangle$): (a-b) dilation rate $\dot{\varepsilon}$, (c-d) shear rate $\dot{\gamma}$, (e-f) pressure p, and (g-h) shear stress τ. Plots (a, c, e, g) are for the radial variations along the direction of motion ($\theta \simeq 0$) whereas plots b, d, f, h are for the azimuthal variations at the radial distance $r \simeq 8d_g$ from the intruder. The vertical dashed lines correspond to the front position $r_c = d/2 + \lambda_c$.

strong peak emerges at low ϕ_0. This result is in agreement with the measured field of the local solid fraction ϕ in the cluster zone which shows a constant plateau value ϕ_p except in a narrow crown around the moving sphere and at the cluster front. Indeed, mass conservation equation, which reads $\phi\dot{\varepsilon} + \mathbf{v} \cdot \nabla\phi = 0$ where $\mathbf{v}$ is the local velocity of the grains, thus leads to $\dot{\varepsilon} \simeq 0$ for $\nabla\phi \simeq 0$ where $\phi = \phi_p$ in the nearly overall cluster (fig. 2a). In the less dense zone close to the moving sphere ($r \simeq d/2$), $\nabla\phi \neq \mathbf{0}$ but is mainly radial and thus normal to $\mathbf{v}$ which is here mainly azimuthal, so that $\mathbf{v} \cdot \nabla\phi \simeq 0$ which again leads to $\dot{\varepsilon} \simeq 0$. By contrast $\mathbf{v} \cdot \nabla\phi \neq 0$ at the cluster front ($r \simeq r_c$) where $\nabla\phi \neq 0$ and is now nearly parallel to $\mathbf{v} \simeq V_0$, so that a significative peak of non-zero $\dot{\varepsilon}$ appears here. This peak is higher for smaller ϕ_0 values as $\dot{\varepsilon}d_g/V_0$ is expected here to scale with $\phi_c - \phi_0$. We can conclude that even if the local density presents some spatial variations, the flow can be considered as incompressible in the overall cluster except in a narrow external cluster rim around $r = r_c$.

The corresponding spatial evolutions of the normalized shear rate $\dot{\gamma}d_g/V_0$ as a function of r/d_g and θ are shown in fig. 4c and d respectively. The shear rate is observed to

be maximum close to the moving sphere at $r \simeq d/2$ and then strongly decreases away from it at larger r roughly as $\dot{\gamma} \sim 1/r^2$. At the front of the dense zone ($r \simeq r_c$), a peak of $\dot{\gamma}d_g/V_0$ arises from large velocity gradient in this transition zone, especially when the dense moving zone is of small extension for low ϕ_0 values. This peak almost disappears for a large enough dense zone at high enough ϕ_0 values as for the peak of $\dot{\varepsilon}$ already seen in fig. 4a. The key point is that the maximal shear rate does not depend significantly on the initial solid fraction ϕ_0 neither does its radial decreasing rate. This means that an intrinsic flow appears close to the moving sphere within the cluster zone independently of its possible diverging size. This flow has an intrinsic length scale which is thus independent of ϕ_0 and is of the order of $1d$ and thus of about $10d_g$ for the present size ratio $d/d_g = 10$. This flow zone corresponds to the narrow crown of lower solid fraction $\phi < \phi_p$. Note that we do not observe here the triangular static zone reported by [40] in their experimental granular chute flow around a large disk confined between two glass plates.

Let us now look at the spatial variations of the stresses in fig. 4e-h. As expected, the local pressure p is maximal at the sphere surface in front of the moving sphere ($r \simeq d/2, \theta \simeq 0$) and decreases radially away from it and toward the equator. As the drag force on the intruder was shown to increase linearly with ϕ_0 (fig. 4a), the good rescaling for the stresses should be $\phi_0\rho V_0^2$. This is the case as the maximal value of $p/(\phi_0\rho V_0^2)$ (and $\tau/(\phi_0\rho V_0^2)$ resp.) at the sphere surface is the same whatever ϕ_0. Moreover, all the curves of figs. 4e and f collapse on a same master curve except near the cluster front. The spatial variations of the shear stress τ are very similar to those of the pressure p with always $\tau < p$. The stresses p and τ scale roughly as $1/r$. Note that $\dot{\gamma}, p, \tau$ does not vanish at large r.

6 Local rheology

Let us now consider any possible local relation that may exist between each of the local invariants of the strain rate tensor and stress tensor. As already discussed, we can consider the flow as incompressible ($\dot{\varepsilon} = 0$) within the overall dense cluster zone (except at the cluster rim $r \simeq r_c$) so that we can discard any key role of the dilation rate $\dot{\varepsilon}$ and focus on the possible relations between the three other invariants $\dot{\gamma}, p$ and τ. The strong coupling between τ and p means that the rheological behavior appears to
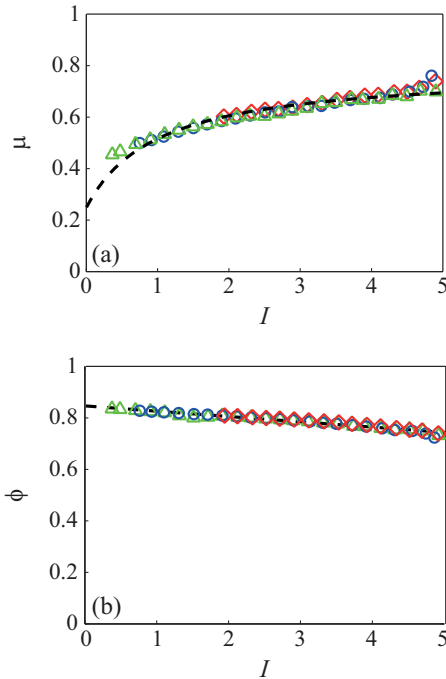
Fig. 6. (Color online). (a) Local friction coefficient $\mu = \tau/p$ and (b) local solid fraction ϕ as a function of the local inertial number I inside the cluster zone for different initial solid fractions ϕ_0. Same data symbols as in fig. 4. (- - -) Fits of equations (a) $\mu = 0.25 + 0.53I/(1 + I)$ and (b) $\phi = 0.846(1 - 0.025I)$.

be of frictional type although no microscopic friction exists in the system. We thus test the possible existence of the local rheology $\mu(I)$ [7] where the local friction coefficient $\mu = \tau/p$ would be linked to the local inertial number $I = \dot{\gamma}d_g/\sqrt{p/\rho\phi}$ related to the local shear rate $\dot{\gamma}$, the local pressure p and local density $\rho\phi$. As τ and p have the same scaling in V_0, the local friction coefficient μ will not depend here on the velocity V_0. Also the local inertial number I that arises in the dense cluster zone will not depend on the intruder velocity V_0 as both $\dot{\gamma}$ and $\sqrt{p}$ scales as V_0. The only spatial variation of I will come from the weak difference of the spatial scalings of $\dot{\gamma}$ and $\sqrt{p}$, together with the weak spatial variation of the local solid fraction ϕ. Figure 5 shows the variations of I in the cluster with (a) the radial position r and (b) the azimuthal position θ relative to the intruder. We see in fig. 5a that I has its highest value of about 5 close to the intruder and decreases away from it following the same master curve whatever the cluster size except at the cluster front. For the largest cluster size ($\phi_0 = 0.75$), we see that I tends towards a non-zero asymptotic value close to $1/2$. Figure 5b shows that there is only weak azimuthal variations of I around the intruder.

In fig. 6a where the local friction coefficient μ is plotted as a function of the local inertial number I, all data collapse in one master curve which means that a local rheology appears in the present flow. A fit through the data by the often used empirical law [11] $\mu = \mu_s + (\mu_2 - \mu_s)I/(I_0 + I)$ works quite well with the values $\mu_s = 0.25 \pm 0.05$, $\mu_2 = 0.78 \pm 0.02$ and $I_0 = 1.0 \pm 0.3$. To describe completely the rheological behavior of the grains in the present flow,

the local solid fraction ϕ inside the cluster is now shown as a function of I in fig. 6b. Again all data collapse on a master curve, which is well described by the linear decrease $\phi = \phi_m(1 - aI)$ with $\phi_m = 0.846 \pm 0.002$ and $a = 0.025 \pm 0.001$. As expected the maximal value ϕ_m found here for ϕ at vanishing I is slightly larger than the plateau value $\phi_p \simeq 0.83$ found previously in the core of the cluster flow. Moreover, ϕ_m value is found very close to the critical value $\phi_c \simeq 0.85$ found for the divergence of λ_c. We believe that ϕ_c and ϕ_m both correspond to the jamming point ϕ_J of the system. The plateau value ϕ_p observed in the cluster core corresponds to the asymptotic minimum value of $I_p \simeq 1/2$ reached in the flow. The observed $\mu(I)$ and $\phi(I)$ variations are very similar to what have been already observed in other granular flow configurations. In the present configuration, the inertial number I that naturally arises is of order one and ranges within only one decade from about 0.5 to 5. As a consequence the local friction coefficient only varies roughly from 0.45 to 0.70 and the local solid fraction roughly from 0.75 to 0.83. The region of high I (high μ and low ϕ) is close to the moving sphere but it is worth noting that I does not vanish far away.

7 Conclusion

Our simulation results show that a steady state regime arises for an intruder sphere moving at constant velocity within a cloud of spherical grains initially at rest and without contact between them and any boundaries. In the present case of dissipative collisions between the grains, a dense cluster of high packing fraction $\phi_p \simeq 0.83$ builds progressively around and reaches a dynamical steady state with a constant size that increases with the initial solid fraction ϕ_0 of the grains and diverges when ϕ_0 approaches the jamming point $\phi_J \simeq 0.85$. The drag force exerted by the grains on the moving sphere increases linearly with ϕ_0 and does not present any diverging behavior close to ϕ_J by contrast to the cluster size. A detailed inspection of the velocity and stress fields inside the cluster reveals that the strongly non-parallel flow can be considered as incompressible inside the overall cluster except at its rim. This flow is observed to be strongly localized within a few grains close to the sphere surface in the direction of motion with a maximal shear rate $\dot{\gamma}$, pressure p and shear stress τ that decreases away. The granular flow is found to obey a local rheology where the local friction coefficient and the local solid fraction are given by the sole inertial number I even if no microscopic friction between the grains is considered here. The scalings of $\dot{\gamma}$, p and τ are such that I does not depend on the flow velocity and varies only by one decade around one inside the overall cluster. This specific behavior originates from the fact that no pressure scale exists in the present configuration that would come from gravity or solid walls, so that the pressure that builds in the system arises from the cluster flow itself. The present simulation results show thus that a local rheology may exist within dense granular materials even for non-parallel flow at least when boundaries do not play any role.

References

1. R.D. Maladen, Y. Ding, C. Li, D.I. Goldman, Science **325**, 314 (2009).
2. H.J. Melosh, *Impact cratering: A geologic process* (1989).
3. J. Blum, G. Wurm, Annu. Rev. Astron. Astrophys. **46**, 21 (2008).
4. W.G. Ellenbroek, M. van Hecke, W. van Saarloos, Phys. Rev. E **80**, 061307 (2009).
5. C. Coulais, R.P. Behringer, O. Dauchot, EPL **100**, 44005 (2012).
6. C. Coulais, A. Seguin, O. Dauchot, Phys. Rev. Lett. **113**, 198001 (2014).
7. GDR MiDi, Eur. Phys. J. E **14**, 341 (2004).
8. F. da Cruz, S. Emam, M. Prochnow, J.N. Roux, F. Chevoir, Phys. Rev. E **72**, 021309 (2005).
9. O. Pouliquen, Phys. Fluids **11**, 542 (1999).
10. P.P. Cortet, D. Bonamy, F. Daviaud, O. Dauchot, B. Dubrulle, M. Renouf, EPL **88**, 14001 (2009).
11. P. Jop, Y. Forterre, O. Pouliquen, Nature **441**, 727 (2006).
12. L. Lacaze, R.R. Kerswell, Phys. Rev. Lett. **102**, 108305 (2009).
13. P.Y. Lagrée, L. Staron, S. Popinet, J. Fluid Mech. **686**, 378 (2011).
14. L. Staron, P.Y. Lagrée, S. Popinet, Eur. Phys. J. E **37**, 5 (2014).
15. M. Bouzid, M. Trulsson, P. Claudin, E. Clément, B. Andreotti, Phys. Rev. Lett. **111**, 238301 (2013).
16. M. Bouzid, M. Trulsson, P. Claudin, E. Clément, B. Andreotti, EPL **109**, 24002 (2015).
17. D. Fenistein, M. van Hecke, Nature **425**, 256 (2003).
18. K.A. Reddy, Y. Forterre, O. Pouliquen, Phys. Rev. Lett. **106**, 108301 (2011).
19. A. Seguin, Y. Bertho, F. Martinez, J. Crassous, P. Gondret, Phys. Rev. E **87**, 012201 (2013).
20. A. Seguin, Y. Bertho, P. Gondret, J. Crassous, Phys. Rev. Lett. **107**, 048001 (2011).
21. A. Amon, V.B. Nguyen, A. Bruand, J. Crassous, E. Clément, Phys. Rev. Lett. **108**, 135502 (2012).
22. V.Y. Zaitsev, P. Richard, R. Delannay, V. Tournat, V.E. Gusev, EPL **83**, 64003 (2008).
23. A. Drescher, G. de Josselin de Jong, J. Mech. Phys. Solids **20**, 337 (1972).
24. D. Bi, J. Zhang, B. Chakraborty, R.P. Behringer, Nature **480**, 355 (2011).
25. A.H. Clark, L. Kondic, R.P. Behringer, Phys. Rev. Lett. **109**, 238302 (2012).
26. A. Seguin, C. Coulais, F. Martinez, Y. Bertho, P. Gondret, Phys. Rev. E **93**, 012904 (2016).
27. S.A. Hall, J. Wright, T. Pirling, E. Ando, D.J. Hughes, G. Viggiani, Granular Matter **13**, 251 (2011).
28. A. Seguin, Y. Bertho, P. Gondret, J. Crassous, EPL **88**, 44002 (2009).
29. S. Takada, H. Hayakawa, J. Engin. Mech., C4016004 (2016).
30. J.J. Moreau, *Unilateral contact and dry friction in finite freedom dynamics* (Springer, 1988).
31. F. Radjaï, F. Dubois, *Discrete-element modeling of granular materials* (Wiley-Iste, 2011).
32. B. Maury, Numer. Math. **102**, 649 (2006).
33. R. Candelier, O. Dauchot, Phys. Rev. Lett. **103**, 128001 (2009).
34. E. Kolb, P. Cixous, N. Gaudouen, T. Darnige, Phys. Rev. E **87**, 032207 (2013).
35. S.R. Waitukaitis, L.K. Roth, V. Vitelli, H.M. Jaeger, EPL **102**, 44001 (2013).
36. Y. Takehara, S. Fujimoto, K. Okumura, EPL **92**, 44003 (2010).
37. Y. Takehara, K. Okumura, Phys. Rev. Lett. **112**, 148001 (2014).
38. M.B. Stone, R. Barry, D.P. Bernstein, M.D. Pelc, Y.K. Tsui, P. Schiffer, Phys. Rev. E **70**, 041301 (2004).
39. A. Ikeda, L. Berthier, P. Sollich, Phys. Rev. Lett. **109**, 018301 (2012).
40. Y. Amarouchene, J.F. Boudet, H. Kellay, Phys. Rev. Lett. **86**, 4286 (2001).